JOURNAL OF GEOPHYSICAL RESEARCH, VOL. 102, NO. C7, PAGES 15,781–15,796, JULY 15, 1997

A unified directional spectrum for long and short wind-driven waves

T. Elfouhaily, B. Chapron, and K. Katsaros
Institut Français de Recherche pour l'Exploitation de la Mer, Plouzané, France

D. Vandemark
NASA Goddard Space Flight Center, Laboratory for Hydrospheric Processes, Wallops Island, Virginia

Abstract. Review of several recent ocean surface wave models finds that while comprehensive in many regards, these spectral models do not satisfy certain additional, but fundamental, criteria. We propose that these criteria include the ability to properly describe diverse fetch conditions and to provide agreement with in situ observations of *Cox and Munk* [1954] and *Jähne and Riemer* [1990] and *Hara et al.* [1994] data in the high-wavenumber regime. Moreover, we find numerous analytically undesirable aspects such as discontinuities across wavenumber limits, nonphysical tuning or adjustment parameters, and noncentrosymmetric directional spreading functions. This paper describes a two-dimensional wavenumber spectrum valid over all wavenumbers and analytically amenable to usage in electromagnetic models. The two regime model is formulated based on the Joint North Sea Wave Project (JONSWAP) in the long-wave regime and on the work of *Phillips* [1985] and *Kitaigorodskii* [1973] at the high wavenumbers. The omnidirectional and wind-dependent spectrum is constructed to agree with past and recent observations including the criteria mentioned above. The key feature of this model is the similarity of description for the high- and low-wavenumber regimes; both forms are posed to stress that the air-sea interaction process of friction between wind and waves (i.e., generalized wave age, u/c) is occurring at all wavelengths simultaneously. This wave age parameterization is the unifying feature of the spectrum. The spectrum's directional spreading function is symmetric about the wind direction and has both wavenumber and wind speed dependence. A ratio method is described that enables comparison of this spreading function with previous noncentrosymmetric forms. Radar data are purposefully excluded from this spectral development. Finally, a test of the spectrum is made by deriving roughness length using the boundary layer model of Kitaigorodskii. Our inference of drag coefficient versus wind speed and wave age shows encouraging agreement with Humidity Exchange Over the Sea (HEXOS) campaign results.

1. Introduction

A reliable statistical description of wind-generated surface waves is of crucial importance for improving understanding of continuous motions and exchanges across the air-sea interface. Satellite remote sensing, engineering design of marine vessels, wave forecasting, and atmosphere-ocean interaction research are all fields where knowledge of the directional wind wave field is needed.

Among statistical descriptions of waves, spectral formulation is generally privileged stemming from the early work of *Phillips* [1958]. There is a wealth of theoretical and empirical studies detailing candidate equilibrium wind wave spectra in the literature [e.g., *Toba*, 1973; *Hasselmann et al.*, 1973; *Mitsuyasu and Honda*, 1974; *Kitaigorodskii et al.*, 1975; *Kahma*, 1981; *Donelan et al.*, 1985; *Phillips*, 1985]. Presently, it is well-accepted that the long-wave spectrum resulting from the Joint North Sea Wave Project (JONSWAP [*Hasselmann et al.*, 1973]) reasonably represents fetch-limited wind wave development. In the high-frequency regime, present models are tenuous in both theory and observation. Extensive attention has been given to both aspects [e.g., *Kitaigorodskii et al.*, 1975; *Phillips*, 1985]. *Banner* [1990] observed that for the full range of wavenumbers, theory and observation remain unreconciled.

It is recognized that for remote sensing studies, precise knowledge of the short-scale wave roughness is the prime requirement. As a first-order approximation, studies often present a spectrum for only high wavenumbers. However, it is now accepted that short waves are intimately coupled with intermediate- and long-scale waves necessitating the need for full wavenumber models such as those developed by *Donelan and Pierson* [1987], *Bjerkaas and Riedel* [1979], and *Apel* [1994]. These models are widely used in microwave radar scattering studies because of their attention to high-frequency spectral definition.

It is our contention that regardless of the means of construction (theoretical or empirical), a wave spectrum should be capable of reproducing certain observations. In the high-frequency regime, integration of the slope spectrum should provide wind-dependent mean square slope results of *Cox and Munk* [1954]. It should also well-represent the dynamics of gravity-capillary wave curvature as seen in laboratory measurements by *Jähne and Riemer* [1990] and by *Hara et al.* [1994]. For long waves, wave age and extended fetch are needed. In addi-

Paper number 97JC00467.
0148-0227/97/97JC-00467$09.00

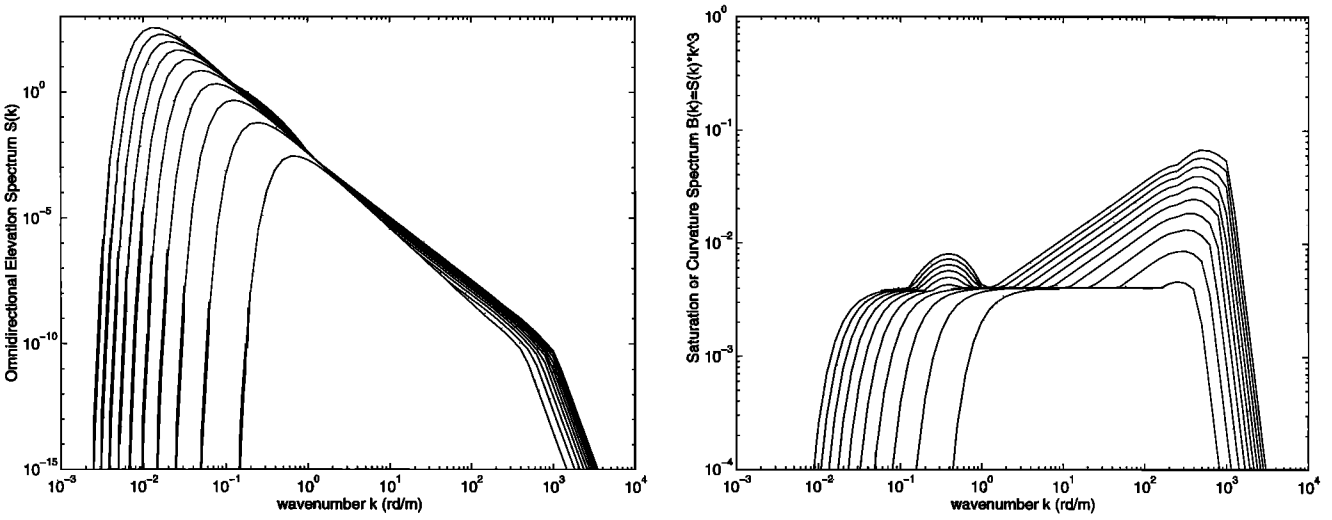

Figure 1. *Bjerkaas and Riedel* [1979] (a) omnidirectional spectrum S^{BR} and (b) curvature spectrum B^{BR} for the full wavenumber range and for wind speeds from 3 m/s (least energetic) to 21 m/s with a 2 m/s step. The secondary gravity-capillary peak is observed for $k_m \sim 370$ rad/m or 1.7 cm wavelength. A sharp spectral cutoff for capillary waves is apparent near 1000 rad/m.

tion, because our interest lies in remote sensing inversion studies, the analytical formulation of the model is crucial. A brief review of several full wavenumber spectra is given in this paper. Remaining difficulties with these proposed spectral forms can be summarized as follows:

1. The *Bjerkaas and Riedel* [1979] spectrum is a composite model with no wave age dependency.
2. The mean square slope inferred from the *Donelan and Pierson* [1987] spectrum does not agree with the *Cox and Munk* [1954] observations.
3. *Apel*'s [1994] spectrum does not agree with the Cox and Munk observations. In addition, we question the placement of the gravity-capillary secondary peak at 0.8 cm for all wind speeds.

As an alternative, we present here a refined spectrum that relies heavily on earlier works but is precise in its agreement with observation and relatively simple in its analytic form. The spectrum is derived strictly for the case of a wind-generated seas, that is, wind and wave direction are aligned. Radar observations are intentionally excluded from the development to limit uncertainties.

This paper is divided into three sections. First, we provide a review of commonly used spectra. Discrepancies between these spectra, especially for the high-frequency region, motivated us to propose a new analytical model. The second part is dedicated to the development of the omnidirectional component of this spectrum. We called our spectrum unified because it features a generalized wave age dependency (u/c) in both long- and short-wave formulations. To extend this spectrum to two dimensions, we desired a spreading function valid over the whole range of wavenumbers and wind speeds. To this end, the last part is a review of existing spreading functions as well as the development of a new spreading function that describes observed upwind-crosswind characteristics. Finally, in the conclusion we provide a new set of parameters that improves the *Donelan and Pierson* [1987] directional spectrum.

2. Bjerkaas and Riedel [1979] Spectrum

The *Bjerkaas and Riedel* [1979] spectrum (S^{BR}) (and its subsequent versions) is widely used in the literature, especially for its ability to satisfy most of available surface displacement measurements based on open ocean data for low frequencies and wind wave tank data for high frequencies. This spectrum is defined in four separate wavenumber ranges. The first spectral range, near the spectral peak of gravity waves, corresponds to the *Pierson and Moskowitz* [1964] spectrum (S^{PM}). Gravity and short-gravity waves are from *Pierson* [1976], while small-gravity to gravity-capillary waves are from *Kitaigorodskii* [1983] and *Leykin and Rosenberg* [1984]. Finally, the capillary wave range is modeled by means of the slope spectra measured by *Cox* [1958]. Bjerkaas and Riedel connected these model spectra by adjusting different arbitrary constants to match curves at the limits between segments. A drawback of this spectrum is the number (five) of wind dependent tuning parameters needed to insure continuity between the spectral segments. In addition, only fully developed sea conditions can be reproduced with this model. Figures 1a and 1b illustrate the omnidirectional spectrum (S^{BR}) and the curvature spectrum ($B^{BR} = k^3 S^{BR}$, see the appendix for definitions), respectively, for different friction velocities (i.e., for different wind speeds).

Fung and Lee [1982] simplified this spectrum and gave a formulation based on only two spectral regimes: *Pierson and Moskowitz* [1964] for gravity waves and *Pierson* [1976] for gravity-capillary waves.

3. Donelan and Pierson [1987] Spectrum

In the comprehensive model of *Donelan and Pierson* [1987], (S^{DP}) the equilibrium range is again divided in two parts. Gravity waves are described using JONSWAP formulation [*Hasselmann et al.*, 1973]. Shorter waves are theoretically derived by requiring a balance between wind input and local dissipation that occurs through viscous damping and wave breaking. For these short waves, wave-wave interactions are assumed negligible.

3.1. Low-Frequency Spectrum

The low wavenumber part of this spectrum (S_l^{DP}) corresponds to gravity waves having wavenumber up to 10 times the

spectral peak (k_p). This limit was introduced by *Donelan et al.* [1985] and *Leykin and Rozenberg* [1984]. The S_l^{DP} spectrum uses the JONSWAP formulation with a slight modification to account for a spectral slope of -2.5 rather than the familiar slope of -3.0. This modification is as simple as multiplying the JONSWAP spectrum by an additional k-dependent factor, the square root of k/k_p.

We reproduce hereafter the formulation of the low-frequency spectrum in terms of wavenumber, although it was originally given in frequency by *Donelan et al.* [1985]. These formulas will also be used throughout this article. For S_l^{DP}, the omnidirectional curvature spectrum of long waves is given by

$$B_l^{DP} = \tfrac{1}{2}\alpha_p L_{PM} J_p \sqrt{k/k_p} \tag{1}$$

where

- S_l^{DP} omnidirectional gravity wave spectrum, equal $k^{-3}B_l^{DP}$;
- α_p rear face or Phillips and Kitaigorodskii equilibrium range parameter;
- k_p wavenumber of the spectral peak;
- L_{PM} Pierson-Moskowitz shape spectrum;
- J_p peak enhancement or "overshoot" factor introduced by *Hasselmann et al.* [1973].

These functions and parameters are defined as follows;

$$L_{PM} = \exp\{-\tfrac{5}{4}(k_p/k)^2\} \tag{2}$$

$$J_p = \gamma^{\Gamma} \tag{3}$$

The latter carries an inverse wave age $\Omega = U_{10}/c_p$ dependency where U_{10} is the wind speed at a height of 10 m above the water surface and c_p is the phase speed of the dominant long wave.

$$\gamma = 1.7 \qquad 0.84 < \Omega_c < 1$$

$$\gamma = 1.7 + 6\log(\Omega_c) \qquad 1 < \Omega_c < 5$$

$$\Gamma = \exp\left\{-\frac{\left(\sqrt{\frac{k}{k_p}} - 1\right)^2}{2\sigma^2}\right\}, \qquad \sigma = 0.08[1 + 4\Omega_c^{-3}]$$

$$\alpha_p = 0.006\Omega_c^{0.55} \qquad 0.84 < \Omega_c < 5$$

$$k_p = k_0\Omega_c^2 \qquad k_0 = g/U_{10}^2$$

with g the acceleration due to gravity.

$$\Omega_c = \Omega\cos(\bar{\theta})$$

where $\bar{\theta}$ is the angle between the wind and the dominant waves at the spectral peak; $\bar{\theta}$ is taken to be close to zero in our study.

Hasselmann et al. [1973] and *Donelan et al.* [1985] relate the inverse wave age to the dimensionless fetch X by an empirical power law based on field observations:

$$\Omega_c^H = 22X^{-0.33} \qquad \Omega_c^D = 11.6X^{-0.23} \tag{4}$$

$X = k_0 x$, where x is the dimensional fetch in meters. Seas are said to be fully developed, mature and young when Ω_c has values close to 0.84, 1.0, and >2.0, respectively. Equation (4) has an asymptotic value of zero for large fetches, a nonphysical result. Therefore S_l^{DP} is only valid for short fetches. An improvement of (4) is provided in section 5.2.1.

3.2. High-Frequency Spectrum

To derive their short-wave spectrum, *Donelan and Pierson* [1987] follow the propagation theory of the spectral energy density as described by *Hasselmann et al.* [1973]. The action spectral density ($\mathcal{A}$) of the wave field may be introduced according to

$$\mathcal{A}(k, \varphi) = c\Psi(k, \varphi) \tag{5}$$

where c is the phase speed and Ψ is the directional spectrum of the short surface waves.

On the basis of the radiative transfer equation, changes in wave action spectral density are described by [e.g., *Phillips*, 1977]

$$\frac{\partial \mathcal{A}}{\partial t} + \mathbf{V}_g \nabla \mathcal{A} = S_{in} + S_{nl} + S_{dis} \tag{6}$$

In the left-hand side of (6), one recognizes in order, the time partial derivative of action spectral density, the wave group velocity and the gradient of $\mathcal{A}$ with respect to spatial horizontal vector $\mathbf{r}$.

The right-hand side of (6) consists of three "source" terms related to wind input, nonlinear effects introduced by, for instance, wave-wave interactions, and energy dissipation mainly dominated by viscosity, breaking and bottom friction, respectively.

Consider the situation of a steady wind blowing horizontally over the water surface, the action spectral density tends to be constant in such a stationary case. As a consequence, the first time derivative term in the energy balance equation vanishes. However, the gradient of $\mathcal{A}$ (second term in (6)) can only be neglected for short waves since it expresses wave advections which are not negligible for long waves. Then, but only for short waves, (6) simplifies to the "equilibrium" or spectral balance case where

$$S_{in} + S_{nl} + S_{dis} = 0 \tag{7}$$

Donelan and Pierson [1987] stated further assumptions; in addition to using a perturbation approach and an additive property of source terms, they neglected the wave-wave interaction and bottom friction. Equation (7) then leads to

$$S_{in} + S_{br} + S_{vis} = 0 \tag{8}$$

where S_{br} and S_{vis} are wave breaking and viscous dissipation terms.

The wind input source term S_{in}, taken from *Miles'* [1957, 1959] theory indicates that wave amplitude grows exponentially:

$$S_{in} = \beta\mathcal{A} \tag{9}$$

where β is the exponential growth rate. This latter is wind-vector-dependent for each spectral wavenumber. Exponential behavior is also implied for viscous damping of the capillary waves as theoretically explained by *Lamb* [1932], namely,

$$S_{vis} = -D\mathcal{A} \tag{10}$$

where $D = 4\nu k^2$ is the exponential viscous decay of the action spectral density and ν is the kinematic viscosity of water.

A defining component of the *Donelan and Pierson* [1987] model for the high-frequency spectrum is their handling of dissipation through wave breaking. This term is taken to be an exponential function of the curvature spectrum B:

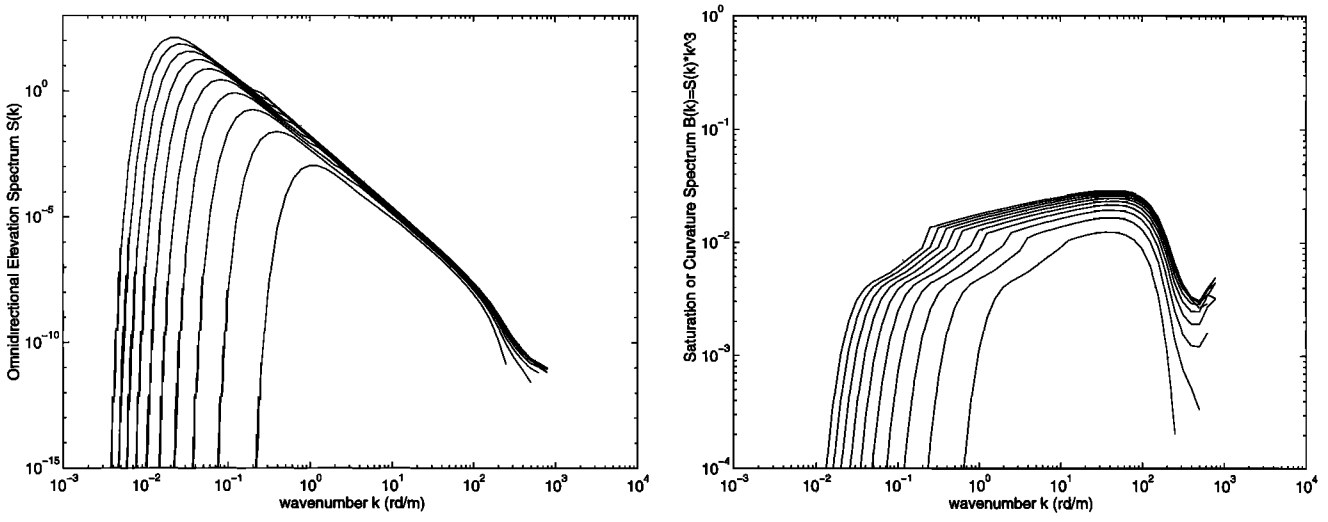

Figure 2. Fully developed *Donelan and Pierson* [1987] (a) omnidirectional spectrum S^{DP} and (b) curvature spectrum B^{DP} for the full wavenumber range and for wind speeds from 3 to 21 m/s with a 2 m/s step. The secondary gravity-capillary peak is located at a wavenumber below 100 rad/m and an abrupt discontinuity occurs at $10k_p$. The increase of the curvature spectrum at high wavenumbers is an artifact caused by the absolute value in (17).

$$S_{\mathrm{br}} = -(\omega\alpha B^n)\mathcal{A} \tag{11}$$

where n and α are unknown functions. The Donelan and Pierson spectrum is then built with

$$n = (n_1 - n_2)\left|\frac{k^2 - k_m^2}{k^2 + k_m^2}\right|^b + n_2 \qquad n_1 = 5,\ n_2 = 1.15 \tag{12}$$

and

$$\ln\alpha = (\ln\alpha_1 - \ln\alpha_2)\left|\frac{k^2 - k_m^2}{k^2 + k_m^2}\right|^b + \ln\alpha_2 \tag{13}$$

$$\ln\alpha_1 = 22,\ \ln\alpha_2 = 4.6,\ b = 3$$

The constants in (12) and (13) have been determined from gravity wave observations and from Ku-band radar backscatter measurements of gravity-capillary waves. Here $k_m = 370$ rad/m is the wavenumber corresponding to waves of 1.7 cm wavelength. These constants should also insure continuity between the low- and the high-wavenumber regimes.

By combining (8)–(11), the directional spectrum of short waves is simply

$$\Psi_h^{\mathrm{DP}}(k, \varphi) = \sqrt[n]{\left|\frac{\beta(k, \varphi) - D(k)}{\alpha\omega}\right|}\, k^{-4} \tag{14}$$

Rather than employing the often-cited wave-growth parameter introduced by *Plant* [1982]

$$\beta/\omega = (0.04 \pm 0.02)(u^*/c)^2 \cos\varphi \tag{15}$$

the wind forcing for short waves is obtained from a quadratic fit of *Larson and Wright*'s [1975] data, as

$$\frac{\beta}{\omega} = 0.194\,\frac{\rho_a}{\rho_w}\left\{\frac{u(\pi/k)\cos\varphi}{c(k)} - 1\right\}^2 \tag{16}$$

where u is the wind speed at a height of $\lambda/2$ from a wave of wavelength λ and c is the corresponding phase speed. The quantities ρ_a and ρ_w are volume density for air and water, respectively.

The azimuthal energy spread of (16) unrealistically excludes angles close to $\pm\pi/2$. To permit the spread of energy around to the crosswind direction and even beyond it, *Donelan and Pierson* [1987] dropped the cosine dependence in (16). This leaves all azimuthal dependence with the definition of a spreading function that is identical for short and long waves. They used the hyperbolic secant for its well-known tractable integrability.

Consequently, the omnidirectional spectrum for high wavenumbers becomes

$$B_h^{\mathrm{DP}}(k) = \frac{1}{\Phi_{\max}}\sqrt[n]{\left|\frac{\beta(k) - D(k)}{\alpha\omega}\right|} \tag{17}$$

where $\Phi_{\max}$ is the maximum of the applied spreading function.

Then, the full omni-directional spectrum reads:

$$S^{\mathrm{DP}}(k) = \begin{bmatrix} k^{-3}B_l^{\mathrm{DP}} & k < 10k_p \\ k^{-3}B_h^{\mathrm{DP}} & k > 10k_p \end{bmatrix} \tag{18}$$

Figure 2 shows the fully developed *Donelan and Pierson* [1987] omnidirectional spectrum S^{DP} (Figure 2a) and its curvature spectrum B^{DP} (Figure 2b). An increase of the degree of saturation for wavenumbers beyond the spectral cutoff is observed in Figure 2b. This is an artifact of the spectral formulation caused by the absolute value in (17).

4. Apel [1994] Spectrum

Apel [1994] developed an analytically simple full spectral model to permit electromagnetic computations. This analytical "improved" spectrum was derived for validity across the entire range of ocean waves. It gathered together spectral branches already modeled by many investigators and integrated new laboratory data especially in the gravity-capillary wave region. Apel called his spectrum the "Donelan-Banner-Jähne" spectrum because of the spreading function made up to match the one from *Donelan et al.* [1985], the omnidirectional spectral slope to be (−4) from *Banner* [1990], and finally the placement of curvature spectral level of the secondary gravity-capillary

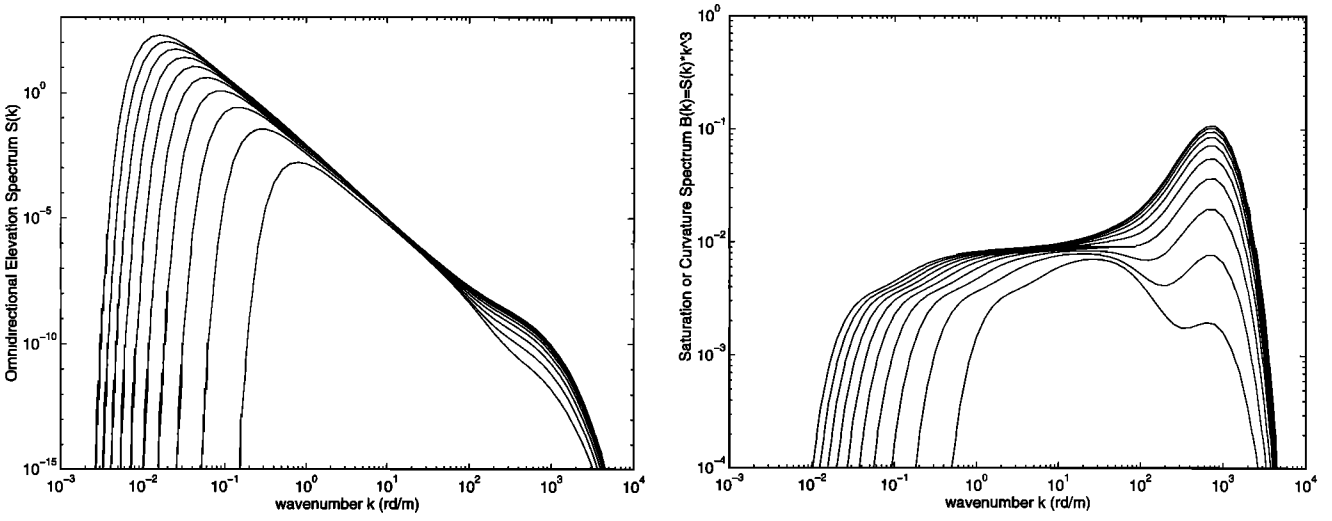

Figure 3. *Apel* [1994] (a) omnidirectional spectrum S^A and (b) curvature spectrum B^A for the full wavenumber range and for wind speeds from 3 up to 21 m/s with a 2 m/s step. The secondary gravity-capillary peak is at 750 rad/m (or 8 mm wavelength).

peak at 750 rad/m from laboratory measurement of *Klinke and Jähne* [1992].

Apel [1994] wrote the final form of his omnidirectional spectrum as

$$S(k) = Ak^{-3}L_{\mathrm{PM}}J_p[R_{\mathrm{ro}} + sR_{\mathrm{res}}]V_{\mathrm{dis}}I_D \qquad (19)$$

where

- A spectral constant that has been chosen as 0.00195 to fit wave height variance or significant wave height observations;
- L_{PM} Pierson-Moskowitz shape spectrum (2);
- J_p JONSWAP peak enhancement (3);
- R_{ro} low-pass quadratic filter with roll-off wavenumber of 100 rad/m as shown by *Klinke and Jähne* [1992] based on tank data;
- s curvature level of an assumed secondary gravity peak at 750 rad/m wavenumber.

$$\log(s) = -4.95 + 3.45\left\{1 - \exp\left(-\frac{U_{10}}{4.7}\right)\right\} \qquad (20)$$

The resonance wavelength is twice smaller than that proposed by *Bjerkaas and Riedel* [1979] and that used by *Donelan and Pierson* [1987], who state that gravity-capillary waves centered around 1.7 cm wavelength should be amplified. The author justified his point of view by recalling the effect of nonlinear wave-wave interactions that have transition rates one order of magnitude faster for capillary waves than for gravity ones.

Model functions were provided for the resonance gravity-capillary peak, R_{res}, of the curvature spectrum and the dissipation mechanism, V_{dis}, as

$$R_{\mathrm{res}} = ak\ \mathrm{sech}\left(\frac{k - k_{\mathrm{res}}}{k_w}\right) \qquad (21)$$

$$a = 0.8 \qquad k_{\mathrm{res}} = 400 \qquad k_w = 450\ (\mathrm{rad/m})$$

$$V_{\mathrm{dis}} = \exp\{-(k/k_{\mathrm{dis}})^2\} \qquad k_{\mathrm{dis}} = 6283\ \mathrm{rad/m} \qquad (22)$$

I_D in (19) is an additional function that appears as a result from integration of the vector spectrum over the azimuth direction,

$$I_D = \frac{1}{\sqrt{2\pi}}\phi_s\ \mathrm{erf}\,(z_s) \qquad (23)$$

$$\phi_s = [0.28 + 10(k_p/k)^{1.3}]^{-0.5} \qquad z_s = \pi/\phi_s\sqrt{2}$$

Figure 3 shows realizations of this omnidirectional spectrum S^A (Figure 3a) and its corresponding curvature spectrum B^A (Figure 3b) for several wind speeds. This spectrum places the gravity-capillary peak at 8 mm wavelength.

5. Unified Omnidirectional Spectrum

The shape of surface wave spectra is still under investigation due to the absence of a unified universal form. Figure 4 illustrates how much the spectra presented above differ. Significant differences exist between these spectra and unfortunately, there are further examples that exhibit similar divergence, e.g., Wallops spectrum from *Huang et al.* [1981], *McClain et al.* [1981] and *Sobieski et al.* [1986, 1988]. The analytical spectrum that we construct below attempts to take advantage of spectral developments presented in the previous sections. We follow *Apel*'s [1994] objective of building an analytical spectrum that can be easily used in modeling electromagnetic interactions with the sea surface. Indeed, the primary need of EM models is the autocorrelation of the displacement field or its Fourier transform, i.e., the elevation spectrum.

5.1. Previous Approaches

The *Bjerkaas and Riedel* [1979] spectrum (S^{BR}) is dependent on too many arbitrary constants due to segment matching and level "tuning," which make its use very limited. Although, the *Donelan and Pierson* [1987] spectrum (S^{DP}) seems to be well constructed for the long waves $k < 10k_p$, the short-wave branch is questionable. As a matter of fact, S^{DP} overestimates mean square slopes by a factor of 1.7 [*Donelan and Pierson*,

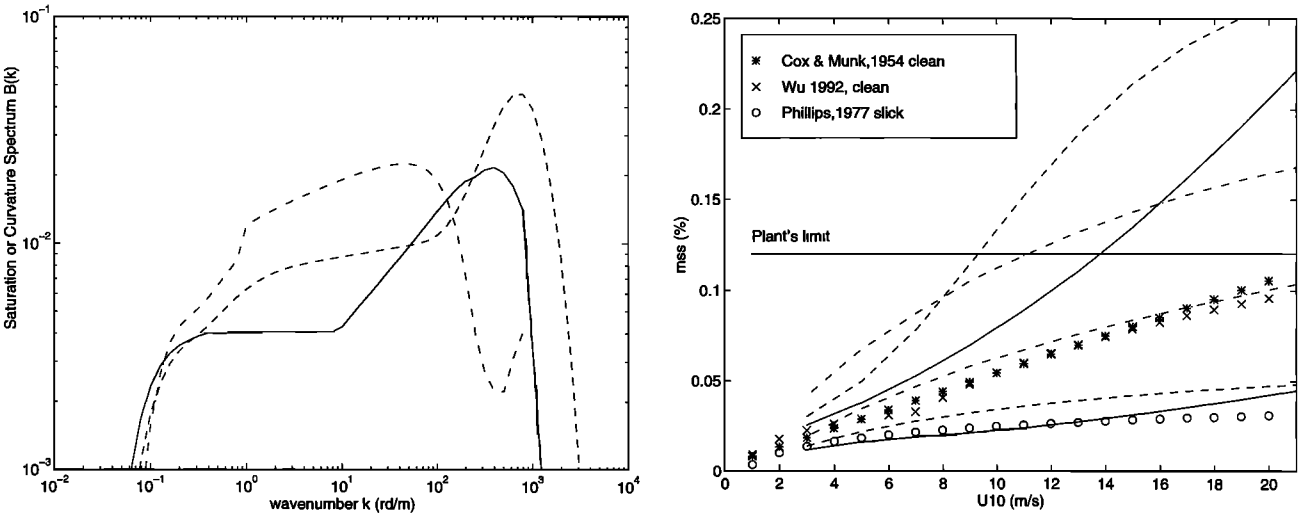

Figure 4. (a) The three presented curvature spectra for a wind speed of 10 m/s. (b) Measured total mean square slopes from *Cox and Munk* [1954] versus mean-square slope (mss) inferred from the three spectra. S^{BR} (solid), S^{DP} (dashed-dotted), and S^{A} (dashed) place the gravity-capillary wave peak at 1.7 cm, 10 cm, 4 cm, and 0.8 cm, respectively.

1987, p. 4984; *Apel*, 1994, p. 16281], compared to the *Cox and Munk* [1954] optical measurements (Figure 4b). The total mean-square slope is highly sensitive to the shape of the spectral tail. *Shemdin and Hwang* [1988] showed discrepancies with the S^{DP} tail by measuring slope frequency spectra up to 300 Hz with a laser-optical sensor. They found that S^{DP} has an early sharp spectral cutoff at frequencies higher than 8 Hz which was not substantiated by their Tower Ocean Wave and Radar Dependence experiment (TOWARD) and Marine Remote Sensing experiment (MARSEN) observations. Those in situ findings suggest that arbitrary parameters (n and α) of the S^{DP} need to be revised. At the end of this paper we propose new constant values that improve the shape of the spectral tail.

Finally, *Apel*'s [1994] spectral model is a relatively simple algebraic form that uses the long-wave spectrum of *Donelan and Pierson* [1987], data and spectral shape of *Banner* [1990] and measurements for gravity-capillary waves of *Jähne and Riemer* [1990]. This composite spectrum has been shown to reproduce the vertically polarized radar field data to within the experimental errors (rms ~ 3 dB). Laser slope gauge data of *Jähne and Riemer* [1990] are reproduced here for completeness in Figure 5a. The degree of saturation of the frequency spectrum $B_f(f) = f^5 S_f(f)$ shows an obvious secondary gravity-capillary peak (f_{peak}) located at about 31 Hz. Hence we are tempted to say that by converting directly this frequency (f_{peak}) to wavenumber (k_{peak}) via the adopted dispersion relationship for long and short waves,

$$\omega^2 = gk\{1 + (k/k_m)^2\} \tag{24}$$

$$k_m = \sqrt{\rho_w g/T} = 370 \text{ rad/m} \qquad \omega = 2\pi f$$

where ρ_w, g, and T are water density, acceleration due to gravity, and water surface tension, respectively; the gravity-capillary secondary peak of curvature spectra would lie around 750 rad/m (~8 mm wavelength). This procedure is obviously wrong. The f_{peak} of the frequency saturation spectrum $B_f(f) = f^5 S_f(f)$ is not simply related to k_{peak} of the wavenumber curvature spectrum $B_k(k) = k^3 S_k(k)$ by the dispersion relationship. The frequency spectrum S_f and the wavenumber spectrum S_k should preserve the total energy after conversion:

$$S_f(f)df = S_k(k)dk \tag{25}$$

Therefore the derivative of the group velocity $V_g = d\omega/dk$ is involved in the total derivative of the wavenumber curvature spectrum $B_k(k) = 2\pi k^3 V_g S_f(f)$.

Figure 5b demonstrates that the Bjerkaas and Riedel spectrum S^{BR}, when correctly expressed in frequency, places the secondary gravity-capillary peak at 31 Hz. We conclude that in contrast to *Apel*'s [1994] suggestions we will continue to place the secondary peak of the curvature spectrum at 370 rad/m (or 1.7 cm wavelength) for all wind speeds. This wavenumber placement is physically consistent because it corresponds to the minimum phase speed where the maximum impact of hydrodynamic and aerodynamic modulations by wind and longer waves must occur [*Smith*, 1990].

Under light wind conditions, an assumption of blockage between gravity and capillary waves may explain the location of the secondary peak near 0.8 cm [e.g., *Zhang*, 1995]. Therefore we do not dismiss the idea of the secondary peak at this placement. Further measurements are required to distinguish the realistic wind speed dependency of this regime.

As often recalled, the most successful measurements of the mean square slope (mss) of the sea surface have been made by *Cox and Munk* [1954]. They evaluated the mss for clean water surface and for a dense artificial slick. Over a clean surface, it is generally accepted that these optical surface measurements provide total integration of the slope spectrum, while, in contrast, wave components shorter than 30 cm are almost entirely absent when considering a dense slick surface. The Cox and Munk linear fit to their data versus wind speed for a clean surface is

$$\text{mss}^{t}_{\text{clean}} = 10^{-3}(3 + 5.12U_{10}) \pm 0.004 \tag{26}$$

$$1 \text{ m/s} < U_{10} < 13 \text{ m/s}$$

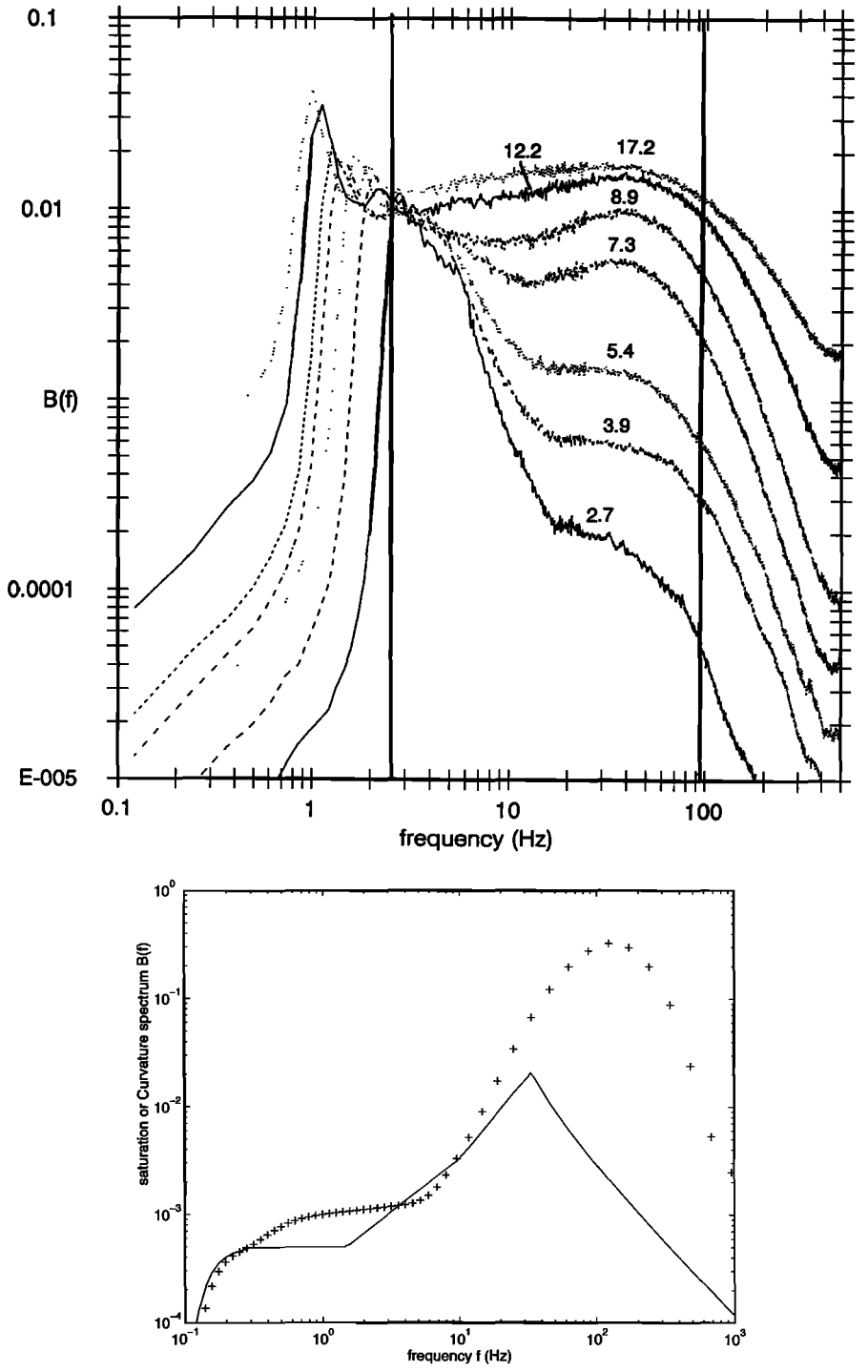

Figure 5. (a) Figure 7 of *Jähne and Riemer* [1990] which depicts measured curvature spectra versus frequency for several values of wind speed given in meters per second. The measured secondary gravity-capillary peak seems to be located between 30 Hz and 40 Hz. (b) Frequency curvature spectra of S^{BR} (solid curve) and S^{A} (pluses) with their secondary peaks placed at 31 Hz and 130 Hz, respectively, for $U_{10} = 10$ m/s.

Wu [1972, 1990] reanalyzed these optical data and showed that a two-regime logarithmic variation is more appropriate for the total mss of the clean surface:

$$\mathrm{mss}^{t}_{\mathrm{clean}} = 10^{-2}\begin{bmatrix} 3.2 + 1.2 \ln (U_{10}/7) & 1 < U_{10} < 7 \text{ m/s} \\ 3.2 + 6 \ln (U_{10}/7) & 7 < U_{10} < 20 \text{ m/s} \end{bmatrix} \quad (27)$$

Phillips [1977] has also argued with the linear dependence and has demonstrated that a logarithmic variation is evident especially for total mss from the artificial slick surface:

$$\mathrm{mss}^{t}_{\mathrm{slick}} = 4.6 \times 10^{-3} \ln (k_s/k_0) \quad (28)$$

$$k_s = 2\pi/0.3 \quad k_0 = g/U_{10}^2$$

Plant [1982] demonstrated that by using a $(u^*/c)^2$ depen-

dency of the growth rate (equation (15)) and the requirement that the momentum flux from wind to waves not exceed the wind stress, the omnidirectional total mean-square slope must be less than $2 \times (0.04 \pm 0.02)$. Thus the upper limit for mean-square slopes of clean surfaces is 0.12, namely,

$$\mathrm{mss}'_{\mathrm{clean}} < 0.12 \tag{29}$$

Equation (27) only reaches this upper limit for a wind speed of 30 m/s. Figure 4b shows the total mss inferred by the three spectra presented above for clean and slick covered surfaces. The *Bjerkaas and Riedel* [1979], the *Donelan and Pierson* [1987], and the *Apel* [1994] spectra all exceed the Plant's limit. So, for those spectra the fractional wave-induced stress will be higher than the total wind stress. This cannot be justified under classical theory. There is no compensating negative stress contribution. *Caudal* [1993] reached a similar conclusion showing that the Donelan and Pierson spectrum and the Plant wave growth expression are not consistent.

5.2. Our Approach

We propose an omnidirectional spectrum expressed as a sum of two spectra regimes:

$$S(k) = k^{-3}[B_l + B_h] \tag{30}$$

where subscripts l and h indicate low and high frequencies, respectively, and B stands for the curvature spectrum ($B = k^3 S$).

5.2.1. Long-wave curvature spectrum. We write here B_l in a general form as

$$B_l = \tfrac{1}{2}\alpha_p \frac{c_p}{c} F_p \tag{31}$$

where α_p is the generalized Phillips-Kitaigorodskii [e.g., *Phillips*, 1977] equilibrium range parameter for long waves dependent on the dimensionless inverse-wave-age parameter $\Omega = U_{10}/c_p$ (U_{10} is the wind speed at a height of 10 m from the water surface), $c(k)$ is the wave phase speed and $c_p = c(k_p)$ is the phase speed at the spectral peak, and F_p is the long-wave side effect function (see below) dependent on dimensionless parameters k/k_p and $\Omega = U_{10}/c_p$.

The long-wave side effect function F_p is given by

$$F_p = L_{\mathrm{PM}} J_p \exp\left\{-\frac{\Omega}{\sqrt{10}}\left[\sqrt{\frac{k}{k_p}} - 1\right]\right\} \tag{32}$$

The first and second terms in (32) are standard *Pierson and Moskowitz* [1964] and JONSWAP peak enhancement functions as given in (2) and (3), respectively. The third term, on the other hand, is an additional cutoff that limits the energy containing part of the spectrum less than $10k_p$. This limitation in spectral roll-off was observed in tank data by *Klinke and Jähne* [1992]. The oscillation of the curvature spectrum (Figure 8b) also created by this fall-off at $10k_p$ was observed by *Leykin et al.* [1984].

The generalized Phillips-Kitaigorodskii equilibrium range parameter for long waves (α_p) is a function of the dimensionless inverse-wave-age parameter $\Omega = U_{10}/c_p$. If one considers, as first approximation, a linear dependency of α_p versus Ω, i.e., $\alpha_p = \alpha_0\Omega$, the corresponding frequency spectrum for gravity waves becomes

$$S_\omega(\omega) = \alpha_0 U_{10} g \omega^{-4} \tag{33}$$

This is in good agreement with measurements of the long-wave fully developed spectrum as reported by *Kahma* [1981] where values of α_0 lie between 4.4×10^{-3} and 6.4×10^{-3}. However, *Donelan et al.* [1985] and *Dobson et al.* [1989], from an extensive data set of developing sea states, reported a nearly square-root Ω dependency. We adopt the functional form for α_p based on their results:

$$\alpha_p = 6 \times 10^{-3}\sqrt{\Omega} \tag{34}$$

The constant 6×10^{-3} is still coherent with Kahma measurements of the equilibrium range for fully developed seas.

Its worth noting that the long-wave spectrum is wave-age-dependent and thus fetch dependent via (4). However, (4) predicts zero inverse wave age as an asymptotic value for infinite fetch. To extend this short fetch relationship to large fetches, *Young et al.* [1994] have shown that total dimensionless energy $\mathscr{E}$ is well represented in deep water by

$$\mathscr{E} = 3.64 \times 10^{-3} \tanh (C_1)^{2.5} \tag{35}$$

$$C_1 = 1.81 \times 10^{-2} X^{0.4}$$

where X is the nondimensional fetch as defined in (4). We combine this result with a dimensionless energy/inverse-wave-age relationship given by *Donelan et al.* [1985] and confirmed by *Dobson et al.* [1989] to arrive at

$$\Omega_c = 0.91 \tanh (C_1)^{-0.75} \tag{36}$$

This relationship has 0.91 as an asymptotic value for large fetch. Since we know that for fully developed seas the inverse wave age should in theory be 0.84, a modification of (36) is needed, and we suggest

$$\Omega_c = 0.84 \tanh \{(X/X_0)^{0.4}\}^{-0.75} \qquad X_0 = 2.2 \times 10^4 \tag{37}$$

This fetch wave-age relationship is compared with JONSWAP *Hasselmann et al.* [1973], *Kahma* [1981], *Donelan et al.* [1985], *Dobson et al.* [1989], and finally, *Young et al.* [1994] relationships in Figure 6a. Overall agreement with former models is obtained.

As an additional check, one can calculate the dimensionless significant wave height as a function of dimensionless fetch:

$$\tilde{H}_s = 0.26 \tanh \{(X/X_0)^{0.4}\}^{1.25} \qquad X_0 = 2.2 \times 10^4 \tag{38}$$

Equation (38) gives, for large fetch values, the standard dimensionless significant wave height of fully developed seas as measured by *Pierson and Moskowitz* [1964] (approximately 0.24). Equation (38) may also be compared, for both short and long fetches, to the model of *Wilson* [1965], who proposed a fit to data observed by a ship-borne wave recorder:

$$\tilde{H}_s^W = 0.3\{1 - (1 + \sqrt{X/X_W})^{-2}\} \qquad X_W = 6.25 \times 10^4 \tag{39}$$

This equation and (38) are in good agreement for X varying from 10^2 up to 10^5 (Figure 6b).

5.2.2. Short-wave curvature spectrum. The high-frequency curvature spectrum, B_h, is expressed as

$$B_h = \tfrac{1}{2}\alpha_m \frac{c_m}{c} F_m \tag{40}$$

where α_m is the generalized Phillips-Kitaigorodskii equilibrium range parameter for short waves dependent on the dimensionless parameter (u^*/c_m), where u^* is the friction velocity at the water surface, c is the short-wave phase speed and

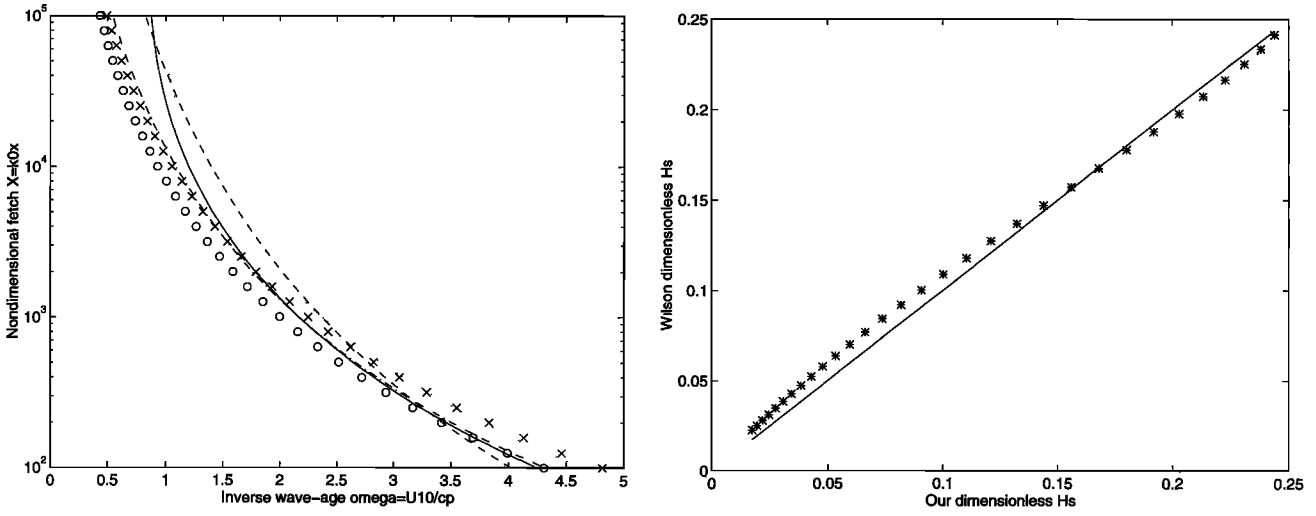

Figure 6. (a) Nondimensional fetch (X) inverse wave age (Ω_c) relationship from *Hasselmann et al.* [1973] (crosses), *Kahma* [1981] (circles), *Donelan et al.* [1985] (dashed curve), *Dobson et al.* [1989] (dashed-dotted curve), *Young et al.* [1994] (dotted curve), and our approximation (solid curve). (b) Compares dimensionless significant wave height model from *Wilson* [1965] (ordinate) to (38) (abscissa). The solid line indicates the one-to-one relationship.

c_m is the minimum phase speed at the wavenumber (k_m) associated with a supposed gravity-capillary peak in the curvature spectrum,

$$c_m = \sqrt{2g/k_m} = 0.23 \text{ m/s}.$$

and F_m is the short-wave side effect function (see below) dependent on dimensionless parameters k/k_m and $\Omega_m = u^*/c_m$.

The short-wave side effect function in (40) is taken here as

$$F_m = \exp\left\{-\frac{1}{4}\left[\frac{k}{k_m} - 1\right]^2\right\} \tag{41}$$

This exponential factor accounts for viscous cutoff and for bandwidth of gravity-capillary waves. As for the α_m parameter, *Phillips* [1985, equation 2.20] developed a theoretical spectrum based on *Plant*'s [1982] growth rate in which he proposed a linear dependence of this equilibrium range on the wind friction velocity over the wave phase speed for small-scale waves. *Phillips* [1985] stated that well inside the equilibrium range, spectral flux divergence, wind input, and dissipation are of equal importance. *Kitaigorodskii* [1983] proposed a similar behavior of the equilibrium range through a Kolmogoroff-type energy cascade mechanism. The wind energy input primarily occurs at the energy-containing scales (i.e., long waves) with dissipation restricted to larger wavenumbers. These theoretical approaches gave a possible explanation for the empirical spectrum of *Toba* [1973]. The Toba-Kitaigorodskii-Phillips curvature spectrum for small-scale waves is given by:

$$B_h(k) = \tfrac{1}{4}\alpha_t \frac{u^*}{c} = \beta I(p) \frac{u^*}{c} \tag{42}$$

where Toba's constant α_t equals 2×10^{-2} and β and $I(p)$ are Phillips' undetermined constants, where p is a spreading parameter introduced by *Phillips* [1985] to generalize the azimuth dependence of the exponential growth rate initially given by *Plant* [1982].

From measurements by *Jähne and Riemer* [1990] and by *Hara et al.* [1994], a linear α_m would be

$$\alpha_m = \alpha_0 \frac{u^*}{c_m} \qquad \alpha_0 = 2 \times 7 \times 10^{-3} \quad c_m = 0.23 \text{ m/s} \tag{43}$$

The constant $\alpha_0 = 1.4 \times 10^{-2}$ compares favorably with the one from *Toba*'s [1973] frequency spectrum $\alpha_t/2 = 1.0 \times 10^{-2}$.

Although, a linear trend appears satisfactory for moderate winds, a departure from measurements is easily noticed (Figure 7a) at both low and high wind speeds. A more accurate fit is obtained by a saturated exponential function as modeled by *Apel* [1994] in (20). However, a two-regime behavior has already been observed and modeled by *Wu* [1972] and *Hwang and Shemdin* [1988] that would correspond to the transition from aerodynamically smooth to rough flow with onset of increased small-scale wave breaking events [*Banner and Melville*, 1976]. Such a transition occurs at $u^* \sim c_m = 0.23$ m/s in their developments. Thus we propose a two-regime logarithmic law for α_m that fits the data of *Jähne and Riemer* [1990] and of *Hara et al.* [1994] (curvature spectral level and friction velocity) as

$$\alpha_m = 10^{-2}\begin{bmatrix} 1 + \ln(u^*/c_m) & \text{for } u^* < c_m \\ 1 + 3\ln(u^*/c_m) & \text{for } u^* > c_m \end{bmatrix} \tag{44}$$

Figure 7a shows comparison between linear (43), exponential (20), and the two-regime logarithmic (44) models. Realizations of our unified omnidirectional spectrum and unified curvature spectrum for the full wavenumber range are shown (Figure 8) where used α_m are from (44). The secondary gravity-capillary peak is at 370 rad/m or 1.7 cm wavelength. This spectrum features a clear saturation of the curvature spectrum for high wind speeds.

6. Angular Spreading Function

6.1. Definitions

In order to separate the unidirectional dependence of the vector spectrum from the angular spread, one can always write

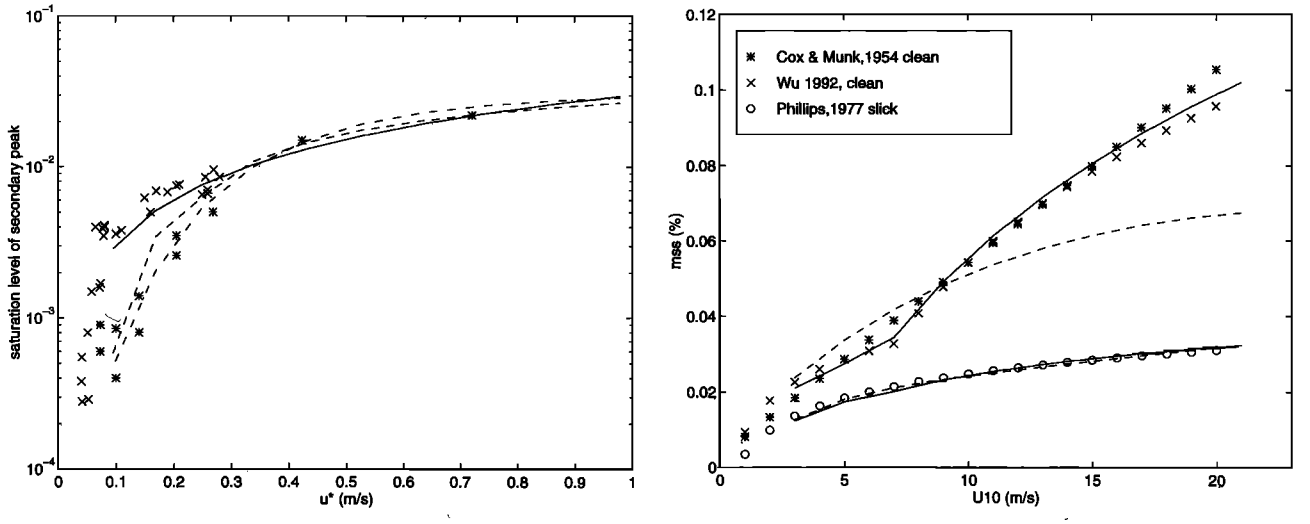

Figure 7. (a) *Jähne and Riemer* [1990] (stars) and *Hara et al.* [1994] (crosses) measurements of the secondary gravity-capillary peak level at 400 rad/m of the curvature spectrum. *Apel* [1994] saturated exponential fit (dashed-dotted curve), our linear approximation (solid curve) and logarithmic model (dashed curve). (b) Comparison of mean square slopes calculated from our unified spectrum (solid curve) and modified *Donelan and Pierson* [1987] (dashed curve) with data from *Cox and Munk* [1954].

$$\Psi(k, \varphi) = \frac{1}{k} S(k)\Phi(k, \varphi) \tag{45}$$

where k is the wave wavenumber and φ is the wave direction relative to the wind. $S(k)$ is the omnidirectional spectrum and Φ is the spreading function defined as

$$\Phi(k, \varphi) = \frac{k\Psi(k, \varphi)}{\int_0^{2\pi} k\Psi(k, \varphi)\, d\varphi} \tag{46}$$

As long as the spreading function is not specified, one still has an exact formulation of the directional spectrum by using (46) in (45).

A directional spectrum is the Fourier transform of the bidimensional covariance of surface displacements, a real and even function. This property of the height covariance is essential in electromagnetic scattering computations and dictates that spreading functions must have a symmetric property regarding the origin, i.e., centrosymmetric property (for more details, see *Guissard* [1993]). Therefore the Fourier series expansion of a spreading function must contain only even harmonics:

$$\Phi(k, \varphi) = \frac{1}{2\pi}\left[1 + \sum_{n=1}^{\infty} a_{2n} \cos(2n\varphi)\right] \tag{47}$$

Unfortunately, noncentrosymmetric spreading functions are widely modeled and used in the literature [*Donelan and Pierson*, 1987; *Apel*, 1994]. This is rather confusing for electromagnetic modelers [*Guissard*, 1993]. To overcome this difficulty,

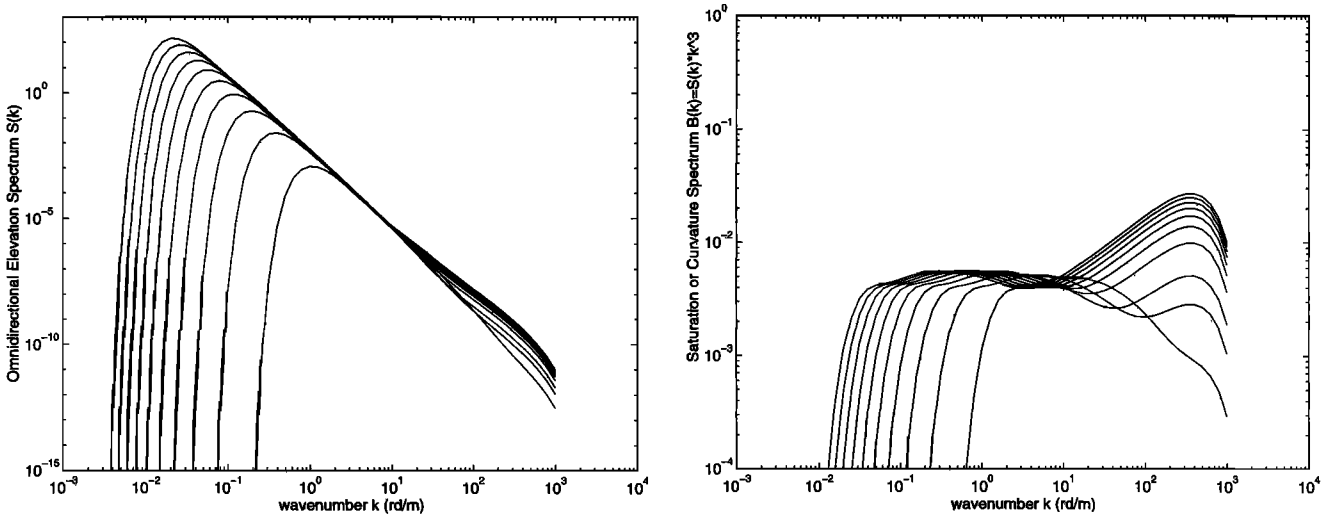

Figure 8. (a) Our unified omnidirectional spectrum S and (b) its corresponding curvature spectrum B for the full wavenumber range and for wind speeds from 3 m/s up to 21 m/s with a 2 m/s step. The secondary gravity-capillary peak is at 370 rad/m or 1.7 cm wavelength.

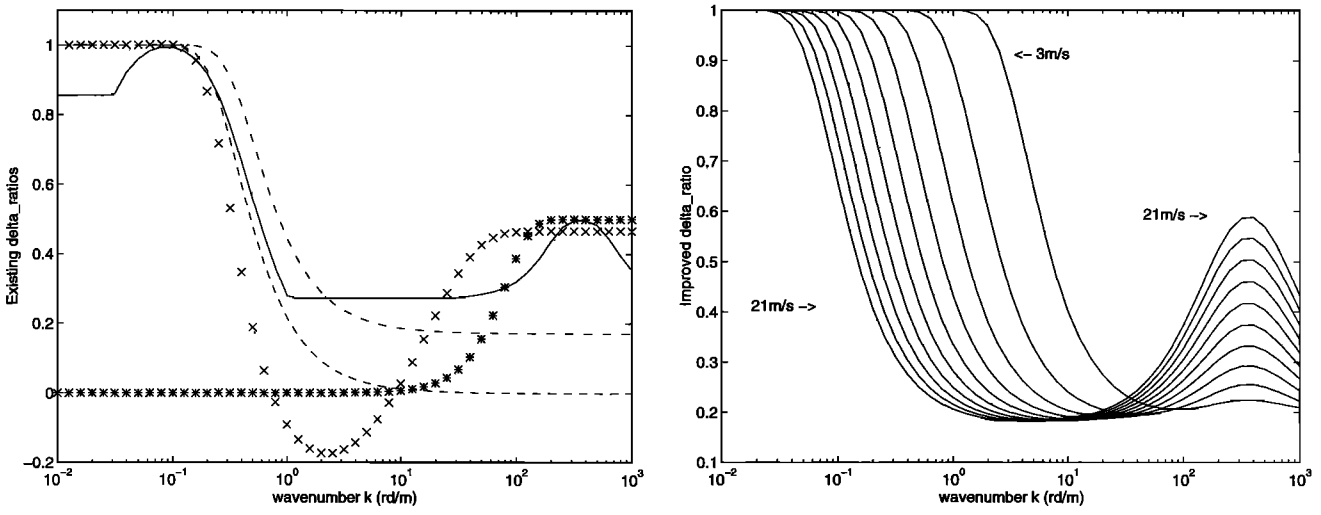

Figure 9. (a) Δ ratio for *Donelan and Pierson* [1987] (solid curve), *Mitsuyasu et al.* [1975] (dashed curve), *Apel* [1994] (dashed-dotted curve), *Fung and Lee* [1982] (stars) and *Nickolaev et al.* [1992] (crosses). (b) Our unified Δ ratio model for wind speed from 3 m/s to 21 m/s with a 2 m/s step.

we define an upwind-crosswind ratio that can be calculated from all symmetric and noncentrosymmetric spreading functions already developed in the past and that transforms those functions to obey (47):

$$\Delta(k) = \frac{\Phi(k, 0) - \Phi\left(k, \frac{\pi}{2}\right)}{\Phi(k, 0) + \Phi\left(k, \frac{\pi}{2}\right)} \tag{48}$$

This Δ ratio parameter is recognizable as the coefficient of the second harmonic when truncating the Fourier series expansion of the angular function; hence

$$\Phi(k, \varphi) = \frac{1}{2\pi}[1 + \Delta(k) \cos(2\varphi)] \tag{49}$$

In the following section, we demonstrate the utility of this upwind-crosswind ratio.

6.2. Existing Spreading Functions

The most popular cosine-shape parametric spreading function was first suggested by *Longuet-Higgins et al.* [1963]

$$\Phi^{LH}(k, \varphi) = G(s) \cos(\varphi/2)^{2s} \tag{50}$$

where the spreading parameter s is, in general, a function of wavenumber (k), wind speed (U_{10}), and inverse wave age Ω_c. The Δ ratio of this function is simply obtained by applying (48) as

$$\Delta(k) = \frac{2^s - 1}{2^s + 1} = \tanh\left(\frac{\ln 2}{2} s\right) \tag{51}$$

Mitsuyasu et al. [1975] proposed first comprehensive estimates of s using measurements from a cloverleaf buoy. We reproduce their expression only in wavenumber for $k > k_p$, although originally given in frequency for the whole frequency range,

$$s = 11.5(c/U_{10})^{2.5} \qquad k > k_p \tag{52}$$

for independent long and short wave developments. By combining (51) and (52), we obtain

$$\Delta^M(k) = \tanh\{3.98(c/U_{10})^{2.5}\} \tag{53}$$

This dependence was later confirmed and improved by *Hasselmann et al.* [1980], who found that a ω/ω_p dependency describes better their pitch-roll buoy data. *Donelan et al.* [1985] found later on that a hyperbolic secant function would fit the observed data even better. Consequently, the Δ ratio of their spreading function reads

$$\Delta^D(k) = \frac{1 - \operatorname{sech}\left(\frac{\pi}{2} h\right)^2}{1 + \operatorname{sech}\left(\frac{\pi}{2} h\right)^2} \tag{54}$$

where h is ω_p/ω dependent. For the sake of simplicity, we will neither further develop (54) nor give the expression of h. However, a numerical evaluation of this Δ ratio is shown in Figure 9.

Apel [1994] proposed an alternative expression to the "sech" function by utilizing *Banner*'s [1990] formulation. He found that a Gaussian spreading function reproduces the observed Donelan-Banner function within modeling errors. We only give here its corresponding Δ ratio:

$$\Delta^A(k) = \tanh\left\{\left(\frac{\pi}{4\phi_s}\right)^2\right\}$$

$$= \tanh\left\{0.173 + 6.168\left(\frac{k_p}{k}\right)^{1.3}\right\} \tag{55}$$

where ϕ_s is given by (23).

We would like to stress that all Δ ratio functions, presented so far, have a hyperbolic tangent form and a ω_p/ω dependency. Accordingly, the Δ ratio decreases with increasing wavenumber. It goes down from 1 for long waves to almost zero for short dispersive waves. Unfortunately, this monotonic decreasing behavior is not satisfactory for a full wavenumber description of

the spreading function. Radar and in situ measurements have suggested distinct directionality for short gravity-capillary waves. We actually believe that short-wave directionality could be emphasized because of the hydrodynamic modulation of short waves by longer ones. Small-scale waves would be less directional if they did not ride on longer directional waves. In order to reproduce radar azimuthal anisotropy, *Fung and Lee* [1982] suggested an increasing Δ ratio across the whole wavenumber range:

$$\Delta^{FL}(k) = a_2[1 - e^{-(k/k_b)^2}] \tag{56}$$

where k_b is the cutoff wavenumber of the high-pass filter ($\lambda_b \sim 8$ cm) and a_2 is wind speed dependent determined from upwind/crosswind mean-square slope asymmetry. This model gave satisfactory results when utilized in microwave modeling. Unfortunately, (56) is not realistic for describing long-wave directionality. It predicts isotropic long waves regardless of wind speed and wave development, i.e., $\Delta^{FL}(k_p) = 0$. For the same purpose, i.e., electromagnetic calculations, *Nickolaev et al.* [1992] gave a similar high-pass filter form except that their exponent involves k instead of k-squared and the cutoff wavelength is almost 5 times higher. In essence, this spreading function is a rather complicated hybrid model between *Longuet-Higgins et al.*'s [1963] cosine form and exponential form of Fung and Lee. For the sake of simplicity, we will not give here the corresponding Δ ratio formula but a numerical realization is shown in our Figure 9a (crosses). Figure 9a shows a comparison between Δ ratios of existing spreading functions for a 10 m/s wind speed and close to fully developed wave system. To date, the shape of the spreading function has been a controversial issue, and no standard form has been given to correctly unify the independent long waves and short-wave developments. Hence a Δ ratio model for the full wavenumber range is yet to be developed.

6.3. Unified Spreading Function

For this model, we assume that long wind waves are aligned with the mean wind direction in steady conditions and the coupling is governed by the $k_p/k \approx (c/c_p)^2$ wavenumber factor. Shorter waves, however, are more dispersive, and a few of them may travel perpendicular to the wind direction. *Donelan et al.* [1985] have argued that some short waves even propagate against the wind (see also *Crombie et al.* [1978] for wave-wave interaction explanation of this phenomenon). Radar observations have shown that short-gravity waves lose their directionality while gravity-capillary waves become more directional. *Shemdin et al.* [1988] have ended up with same conclusions when observing centimeter waves with stereophotography. Owing to the natural involvement of the hyperbolic tangent function and the phase speed ratio in all presented spreading expressions, we propose a unified full wavenumber approach that can be written

$$\Delta(k) = \tanh\{a_0 + a_p(c/c_p)^{2.5} + a_m(c_m/c)^{2.5}\} \tag{57}$$

where a_0 is constant while a_p and a_m are functions of U_{10}/c_p and u^*/c_m, respectively; a_0 is taken to be the minimum value for which the s parameter of *Longuet-Higgins et al.* [1963] in (51) equals 0.5. When looking to long-wave direction measurements from *Mitsuyasu et al.* [1975], *Donelan et al.* [1985], and *Banner* [1990], it turns out that a_p is a constant whose value lies between 4 and 6. For high-frequency waves, the a_m parameter is a function of u^*/c_m and was deduced from mean-square slope asymmetry as measured by *Cox and Munk* [1954]:

$$\Delta\text{mss}_{\text{clean}} = (1.24U_{10} - 3) \times 10^{-3} = \frac{1}{2}\int_0^\infty \Delta(k)S(k)k^2\,dk \qquad U_{10} > 3 \text{ m/s} \tag{58}$$

where Δmss means the difference between mss for a clean surface from upwind and crosswind directions. We then write these functions as

$$a_0 = \frac{\ln(2)}{4} \qquad a_p = 4$$
$$a_m = 0.13\,\frac{u^*}{c_m} \qquad c_m = \sqrt{\frac{2g}{k_m}} = 0.23 \text{ m/s} \tag{59}$$

The wind speed at a height of 10 m was converted to friction velocity under stable conditions by using the neutral drag coefficient formula given by *Garratt* [1977] or by *Wu* [1982] for close to fully developed sea conditions. Figure 10a compares in polar coordinate this unified spreading function at the spectral peak k_p and at the secondary gravity-capillary peak k_m with the *Longuet-Higgins et al.* [1963] spreading function (50) for $s = 2$.

7. Consistency in the Interaction Between Wind and Waves

We have developed the unified spectral model to be consistent with in situ wind and wave observations for both long and short waves. A further fundamental test of the spectrum can be made by examining its consistency within a boundary layer model. Such application entails integration of our wave roughness spectrum to derive the basic near-surface aerodynamic roughness length z_0. This roughness term carries the fundamental relationship between wind speed and friction velocity through the well-known "the law of the wall" equation:

$$U(z) = \frac{u^*}{\kappa}\ln\left(\frac{z}{z_0}\right) \qquad z \gg \delta_v \quad z \gg h_s \tag{60}$$

Further, (60) is often rewritten (assuming a neutral stability assumption) as

$$u^* = \sqrt{Cd_{10N}}\,U_{10} \tag{61}$$

where Cd_{10N} is termed the neutral stability drag coefficient at 10 m above the sea level.

The implication of the preceding comments is that application of our spectrum, with its wind and wave age dependence, will lead to some relationship between wind speed and wind stress for a given wave age. This derivation of the drag coefficient can then be compared with observations. *Kitaigorodskii* [1973] provided a basic surface layer theory detailing two primary length scales in the wind-roughening processes, thickness of the viscous sublayer (δ_v) adjoining an aerodynamically smooth surface,

$$\delta_v = v/u^* \tag{62}$$

where $v = 14 \times 10^{-6}$ m^2/s and "mean height of the roughness protuberances" of an aerodynamically rough moving surface,

$$h_s = \sqrt{\int_0^\infty S(k)\exp(-2\kappa c(k)/u^*)\,dk} \tag{63}$$

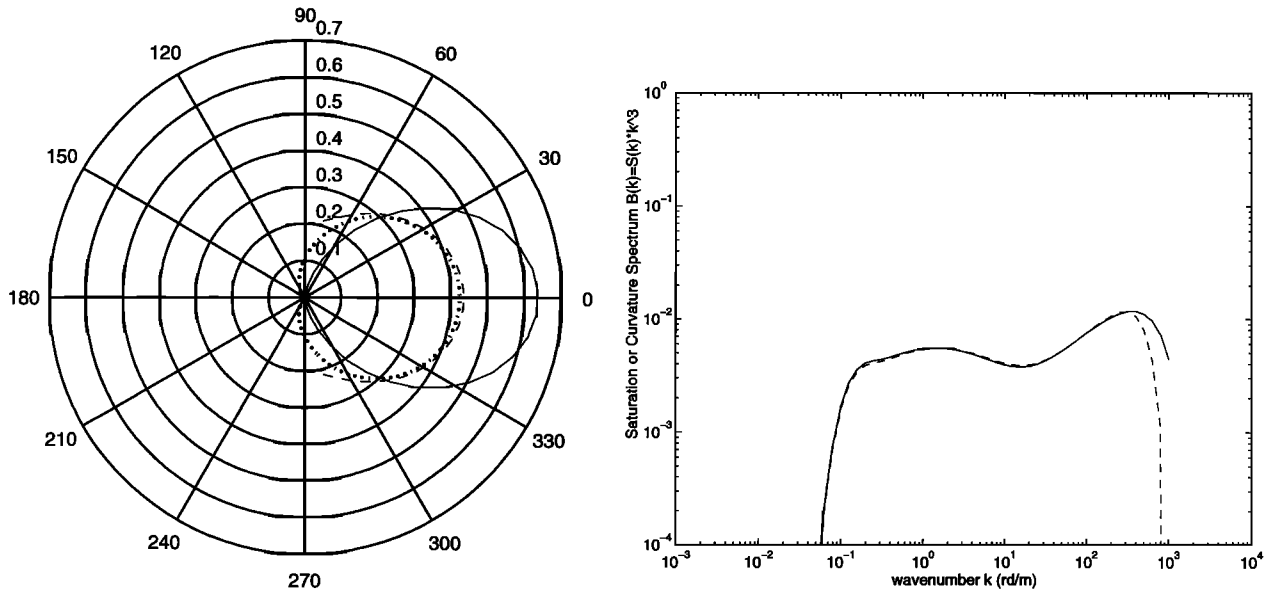

Figure 10. (a) Comparison, in polar coordinate (upwind $\varphi = 0$), of our unified spreading function at the spectral peak k_p (solid curve) and at the secondary gravity-capillary peak k_m (dashed curve) with the *Longuet-Higgins et al.* [1963] cosine-shape spreading function for a spreading parameter of $s = 2$ (dotted curve). Note that the dashed and dotted curves are almost superimposed over must of the angles. (b) A comparison between our spectrum (solid curve) and modified *Donelan and Pierson* [1987] (dashed curve) for a 10 m/s wind speed.

A total aerodynamic roughness parameter z_0 can be simply taken as the sum of "smooth" and "rough" lengths [*Smith*, 1988] reproduced here in Kitaigorodskii's notation:

$$z_0 = A_v \delta_v + A_s h_s \tag{64}$$

Kitaigorodskii [1973] reported that A_v is a universal constant of 0.11. While A_s has values between 0.2 and 0.02. A_s is most likely a function of the sea state. We simply take $A_s = u^*/c_p$ which is compatible with the observations of *Geernaert et al.* [1986].

When using our unified spectrum (30 and its subsequent equations) in the total roughness model (64), we found that frequencies well above the spectral peak of the equilibrium range are responsible for almost all the stress under steady state conditions. Figure 11a illustrates that when the omnidirectional spectrum is multiplied by the *Kitaigorodskii* [1973]

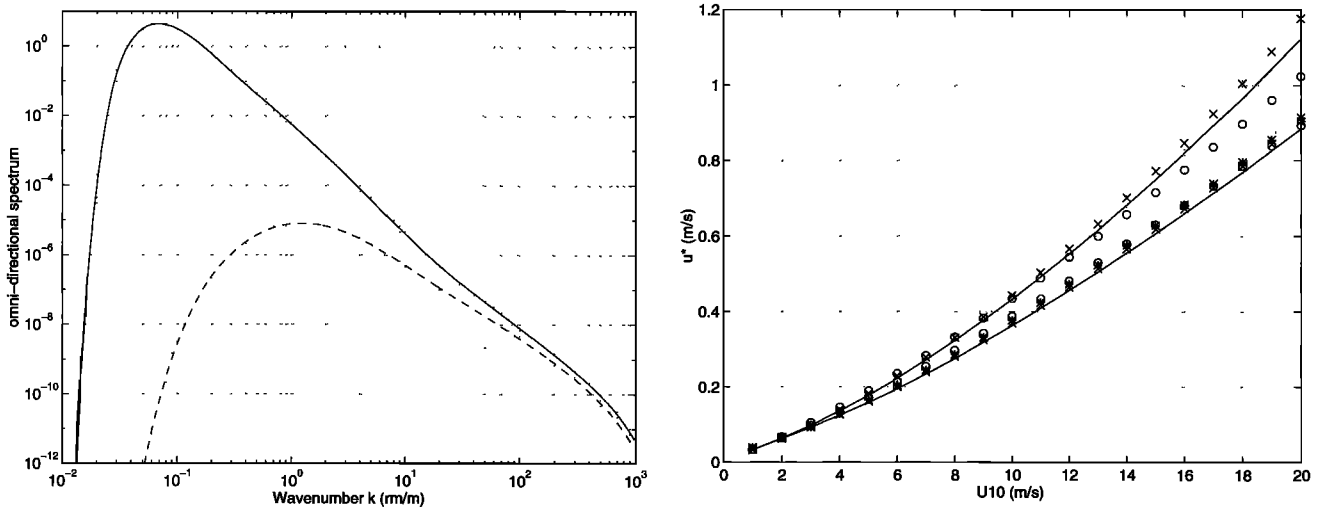

Figure 11. (a) An example of our omnidirectional unified spectrum $S(k)$ (solid curve) and $S(k)$ multiplied by *Kitaigorodskii*'s [1973] exponential term (dashed curve) as in (63). Numerical realization of this example is only performed for wind speed $U_{10} = 10$ m/s and friction velocity $u^* = 0.38$ m/s and inverse wave age ($\Omega = U_{10}/c_p = 0.84$). (b) Wind friction velocity versus wind speed and inverse wave age; our model (64) (solid curve), HEXOS results (65) (crosses), *Donelan et al.* [1993] expression (66) (circles), *Garratt* [1977] model (stars). Note that for $\Omega = 0.84$ all models are similar (bottom set of curves). While for $\Omega = 3.0$ our prediction lies between Donelan's and HEXOS's (top set of curves). These chosen values of the inverse wave age correspond to fully developed and young seas, respectively.

exponential term in (63), only short-gravity and gravity-capillary waves support the total integral term. *Geernaert* [1990] came to the same conclusion when reviewing relevant roughness models. *Makin et al.* [1995] by developing a wave boundary model based on *Miles'* [1957, 1959] and *Janssen's* [1989] theories, concluded that short-gravity waves are responsible for almost all the downward momentum flux.

Maat et al. [1991] and *Smith et al.* [1992] proposed a relationship between the roughness parameter z_0 and the related wave age parameter (u^*/c_p). Their HEXOS results can be summarized (including rms uncertainty of the fit to data) as

$$\frac{gz_0}{u^{*2}} = (0.45 \pm 0.05)\frac{u^*}{c_p} \tag{65}$$

This formulation indicates that young seas (low c_p) are rougher than mature ones (high c_p). Similar results were obtained recently by *Donelan et al.* [1993]. Based on in situ measurements, *Donelan et al.* [1993] proposed however a slightly different model for z_0,

$$z_0 = 3.7 \times 10^{-5}\frac{U_{10}^2}{g}\left(\frac{U_{10}}{c_p}\right)^{0.9} \tag{66}$$

Figure 11a shows friction velocity function of wind speed and wave age as inferred from our unified spectrum by utilizing iterative scheme based on *Kitaigorodskii's* [1973] model (64) and a u^*-U_{10} relationship (61) along with in situ results. Overall agreement can easily be seen with both in situ models and *Garratt's* [1977] model for mature seas. These results strengthen the idea that our unified spectrum is consistent with wind stress measurements.

8. Conclusion

In this paper we have attempted to derive from several recent experimental results a relatively simple closed-form model for the surface wave directional spectrum. The latter has been developed solely from in situ or tank measurements. Thus no radar data have been included in elaborating this model.

Our directional wave spectrum satisfactorily models surface waves from near the main spectral peak up to the gravity-capillary peak. Nondeveloped seas were also modeled by using the modified JONSWAP formulation for long waves together with a new fetch versus wave age relationship that extends its validity to large fetch values in open ocean. The secondary gravity-capillary peak increases with the wind friction velocity as a two-regime logarithmic function as derived from *Jähne and Riemer* [1990] and *Hara et al.* [1994] tank data. The omnidirectional spectral model reproduces significant wave height for developing seas and measured mean square slopes (mss) for both clean and oil-slick covered water surfaces (Figure 7b). Moreover, when combined with our simple spreading function, upwind-crosswind asymmetry also verifies for both clean and slick mss to within experimental errors. By combining all former equations, our improved unified directional spectrum can then be written as

$$\Psi(k, \varphi) = \frac{1}{2\pi}k^{-4}[B_l + B_h][1 + \Delta(k)\cos(2\varphi)] \tag{67}$$

Where B_l, B_h, and Δ are from (31), (40), and (57) and their subsequent formulas. If we use (17) instead of (40) for the omnidirectional curvature spectrum of short waves, one obtains a modified *Donelan and Pierson* [1987] spectrum that improves mss predictions as reported in Figure 7a (dashed curve). With this modification, the curvature secondary peak moves over to 1.7 cm wavelength (Figure 7b). New parameters that improve on the Donelan and Pierson spectrum are suggested here to be, $n + 1 = 3$ from *Phillips* [1985] and $\ln \alpha = n\{(k/k_m - 1)^2 + 4.4\}$ from the current development.

The main feature of our spectrum is the equilibrium range dependence on the generalized wave age (u/c) for which u is the wind speed at a height of 10 m from the water surface (U_{10}) for the long-wave spectral domain [*Kahma*, 1981; *Donelan et al.*, 1985; *Dobson et al.*, 1989] and the friction velocity (u^*) for the short-gravity and gravity-capillary wave spectral domain [*Toba*, 1973; *Kitaigorodskii*, 1983; *Phillips*, 1985]. Short-gravity and gravity-capillary waves are responsible for most of the wave-induced stress. When using our unified spectrum in the boundary layer model proposed by *Kitaigorodskii* [1973], the inferred form drag agrees with HEXOS campaign measurements [*Smith et al.*, 1992]. Therefore our unified spectrum is consistent with wind stress measurements.

The only remote-sensing data used in our development are optical data. Our approach is very flexible and can be used in conjunction with future in situ data to refine these initial findings.

Appendix: Spectral Definitions

By definition, the elevation spectrum is the Fourier transform of the autocovariance function of the surface displacements.

$$\Psi(\mathbf{k}) = \mathrm{FT}\{\langle \eta(\mathbf{r}_0)\eta(\mathbf{r}_0 + \mathbf{r})\rangle\} \tag{A1}$$

FT being the Fourier transform operator, angle bracket are the ensemble average operator, η is the surface elevation with zero mean, and $\mathbf{r}$ is horizontal lag over the surface.

In our analysis, only spatial variability is considered. Temporal or frequency dependence of wave spectra is outside the scope of this study. The directional spectrum is normalized as

$$\sigma_\eta^2 = \langle \eta^2 \rangle = \int_{-\infty}^{\infty}\int_{-\infty}^{\infty}\Psi(k_x, k_y)\,dk_x\,dk_y$$

$$= \int_0^{\infty}\int_{-\pi}^{\pi}\Psi(k, \varphi)k\,dk\,d\varphi = \int_0^{\infty}S(k)\,dk \tag{A2}$$

where σ_η is the standard deviation of surface elevations and $\Psi(k_x, k_y)$ and $\Psi(k, \varphi)$ are directional spectrum in Cartesian and polar coordinates, respectively. The wind is assumed to be blowing in the positive x axis. The omnidirectional spectrum $S(k)$ is

$$S(k) = \int_{-\pi}^{\pi}\Psi(k, \varphi)k\,d\varphi \tag{A3}$$

The mean square slope in the upwind direction is

$$\mathrm{mss}_x = \int_{-\infty}^{\infty}\int_{-\infty}^{\infty}k_x^2\Psi(k_x, k_y)\,dk_x\,dk_y$$

$$= \int_0^{\infty}\int_{-\pi}^{\pi}k^2\cos^2\varphi\Psi(k, \varphi)k\,dk\,d\varphi \tag{A4}$$

Table A1. Spectral Definition and Dimensions

Spectral Name	Form and Symbol	Units	Dimension
Elevation	$S(k)$	m^3/rad	1-D
Slope	$P(k) = k^2S(k)$	$m \times rad$	1-D
Saturation or curvature	$B(k) = k^3S(k)$	rad^2	1-D
Elevation	$\Psi(k_x, k_y)$	m^4/rad^2	2-D
Upwind slope	$P_x = k_x^2\Psi$	m^2	2-D
Crosswind slope	$P_y = k_y^2\Psi$	m^2	2-D
Curvature or saturation	$X(k_x, k_y) = k^4\Psi$	rad^2	2-D

and in the crosswind direction is

$$\text{mss}_y = \int_{-\infty}^{\infty}\int_{-\infty}^{\infty} k_y^2\Psi(k_x, k_y)\, dk_x\, dk_y$$

$$= \int_0^{\infty}\int_{-\pi}^{\pi} k^2 \sin^2\varphi\Psi(k, \varphi)k\, dk\, d\varphi \qquad \text{(A5)}$$

The total mean square slope in omnidirectional context is, therefore,

$$\text{mss} = \text{mss}_x + \text{mss}_y = \int_{-\infty}^{\infty}\int_{-\infty}^{\infty} (k_x^2 + k_y^2)\Psi(k_x, k_y)\, dk_x\, dk_y$$

$$= \int_0^{\infty}\int_{-\pi}^{\pi} k^2\Psi(k, \varphi)k\, dk\, d\varphi = \int_0^{\infty} k^2S(k)\, dk \qquad \text{(A6)}$$

The factor in the final integral ($k^2S(k)$) is called the omnidirectional slope spectrum.

The saturation spectrum is defined in order to remove the k^{-3} behavior in omnidirectional spectrum and the k^{-4} dependence for directional spectral according to *Phillips'* [1977] theory. The saturation spectrum is commonly called the curvature spectrum. Table A1 summarizes the previous definitions and gives their respective dimension and units.

Acknowledgments. The authors would like to thank colleagues over IFREMER for the helpful comments and valuable discussions. Among then we specially thank Laurent Dupont, Robert Ezraty, Jerôme Gourrion, and Vincent Kerbaol.

References

Apel, J. R., An improved model of the ocean surface wave vector spectrum and its effects on radar backscatter, *J. Geophys. Res.*, *99*, 16,269–16,291, 1994.

Banner, M. L., Equilibrium spectra of wind waves, *J. Phys. Oceanogr.*, *20*, 966–984, 1990.

Banner, M. L., and W. K. Melville, On the separation of air-flow over water waves, *J. Fluid Mech.*, *77*, 825–842, 1976.

Bjerkaas, A. W., and F. W. Riedel, Proposed model for the elevation spectrum of a wind-roughened sea surface, *Tech. Rep. APL-TG-1328-I-31*, 31 pp., Appl. Phys. Lab., Johns Hopkins Univ., Laurel, Md., 1979.

Caudal, G., Self-consistency between wind stress, wave spectrum and wind-induced wave growth for fully rough air-sea interface, *J. Geophys. Res.*, *98*, 22,743–22,752, 1993.

Cox, C., Measurements of slopes of high frequency waves, *J. Mar. Res.*, *16*, 199–225, 1958.

Cox, C. S., and W. H. Munk, Statistics of the sea surface derived from Sun glitter, *J. Mar. Res.*, *13*, 198–227, 1954.

Crombie, D. D., K. Hasselmann, and W. Sell, High-frequency radar observations of sea waves traveling in opposition to the wind, *Boundary Layer Meteorol.*, *13*, 45–54, 1978.

Dobson, F., W. Perrie, and B. Toulany, On the deep-water fetch laws for wind-generated surface gravity waves, *Atmos. Ocean*, *27*(1), 210–236, 1989.

Donelan, M. A., and W. J. P. Pierson, Radar scattering and equilibrium ranges in wind-generated waves with application to scatterometry, *J. Geophys. Res.*, *92*, 4971–5029, 1987.

Donelan, M. A., J. Hamilton, and W. H. Hui, Directional spectra of wind generated waves, *Philos. Trans. R. Soc. London, Ser. A*, *315*, 509–562, 1985.

Donelan, M. A., F. W. Dobson, S. D. Smith, and R. J. Anderson, On the dependence of sea surface roughness on wave development, *J. Phys. Oceanogr.*, *23*, 2143–2149, 1993.

Fung, A. K., and K. K. Lee, A semi-empirical sea-spectrum model for scattering coefficient estimation, *IEEE J. Oceanic Eng.*, *OE-7*(4), 166–176, 1982.

Garratt, J. R., Review of drag coefficients over oceans and continents, *Mon. Weather Rev.*, *105*, 915–929, 1977.

Geernaert, G. L., Bulk parameterization for the wind stress and heat fluxes, in *Surface Waves and Fluxes*, edited by G. L. Geernaert and W. J. Plant, pp. 91–172, Kluwer Acad., Norwell, Mass., 1990.

Geernaert, G. L., K. B. Katsaros, and K. Richter, Variations of the drag coefficient and its dependence on sea state, *J. Geophys. Res.*, *91*, 7667–7679, 1986.

Guissard, A., Directional spectrum of the sea surface and wind scatterometry, *Int. J. Remote Sens.*, *14*(8), 1615–1633, 1993.

Hara, T., E. J. Bock, and D. Lyzenga, In situ measurements of capillary-gravity wave spectra using a scanning laser slope gauge and microwave radars, *J. Geophys. Res.*, *99*, 12,593–12,602, 1994.

Hasselmann, K., et al., Measurements of wind-wave growth and swell during the Joint North Sea Wave Project (JONSWAP), *Dtsch. Hydrogr. Z.*, *12*, 95 pp., 1973.

Hasselmann, D. E., M. Kunckel, and J. A. Ewing, Directional wave spectra observed during JONSWAP 1973, *J. Phys. Oceanogr.*, *10*, 1264–1280, 1980.

Huang, N., S. R. Long, Chi-Chao, T., Y. Yuen, and F. L. Bliven, A unified two-parameter wave spectral model for a general sea state, *J. Fluid Mech.*, *112*, 203–224, 1981.

Hwang, P. A., and O. H. Shemdin, The dependence of sea surface slope on atmospheric stability and swell conditions, *J. Geophys. Res.*, *93*, 13,903–13,912, 1988.

Jähne, B., and K. S. Riemer, Two-dimensional wave number spectra of small-scale water surface waves, *J. Geophys. Res.*, *95*, 11,531–11,546, 1990.

Janssen, P. A. E. M., Wave induced stress and the drag of air flow over sea waves, *J. Phys. Oceanogr.*, *19*, 745–754, 1989.

Kahma, K., A study of the growth of the wave spectrum with fetch, *J. Phys. Oceanogr.*, *11*, 1503–1515, 1981.

Kitaigorodskii, S. A., *The Physics of Air-Sea Interactions*, pp. 9–73, Keter Press, Jerusalem, 1973.

Kitaigorodskii, S. A., On the theory of the equilibrium range in the spectrum of wind-generated gravity waves, *J. Phys. Oceanogr.*, *13*, 816–827, 1983.

Kitaigorodskii, S. A., V. P. Krasitskii, and M. M. Zaslavskii, On Phillips' theory of equilibrium range in the spectra of wind-generated gravity waves, *J. Phys. Oceanogr.*, *5*, 410–420, 1975.

Klinke, J., and B. Jähne, 2D wave number spectra of short wind waves—Results from wind wave facilities and extrapolation to the ocean, *SPIE Proc.*, *1749*, 1–13, 1992.

Lamb, H., *Hydrodynamics*, 6th ed., 783 pp., Cambridge Univ. Press, New York, 1932.

Larson, T. R., and J. W. Wright, Wind-generated gravity-capillary waves: Laboratory measurements of temporal growth rates using microwave backscatter, *J. Fluid Mech.*, *70*, 417–436, 1975.

Leykin, I. A., and A. D. Rosenberg, Sea-tower measurements of wind-wave spectra in the Caspian Sea, *J. Phys. Oceanogr.*, *14*, 168–176, 1984.

Leykin, I. A., K. V. Pokazeyev, and A. D. Rozenberg, Growth and saturation of wind waves in a laboratory channel, *Atmos. Ocean. Phys.*, *20*(4), 313–318, 1984.

Longuet-Higgins, M. S., On the dynamics of steep gravity waves in deep water, *Turbulent Fluxes Through the Sea Surface, Wave Dynam-*

ics, and Prediction, edited by A. Favre, and K. Hasselmann, *NATO Conf. Ser., Ser. V, 1*, 199–220, 1978.

Longuet-Higgins, M. S., D. E. Cartwright, and N. D. Smith, Observations of the directional spectrum of sea waves using the motions of a flotation buoy, in *Ocean Wave Spectra*, pp. 111–136, Prentice-Hall, Englewood Cliffs, N. J., 1963.

Maat, N., C. Kraan, and W. A. Oost, The roughness of wind waves, *Boundary Layer Meteorol., 54*, 89–103, 1991.

Makin, V. K., V. N. Kudryavtsev, and C. Mastenbroek, Drag of the sea surface, *Boundary Layer Meteorol., 73*, 159–182, 1995.

McClain, C. R., D. T. Chen, and W. D. Hart, Surface wave statistics and spectra during high sea state conditions in the North Atlantic, Nav. Res. Lab., Washington, D. C., Dec. 30, 1981.

Miles, J. W., On the generation of surface waves by shear flows, *J. Fluid Mech., 3*, 185–204, 1957.

Miles, J. W., On the generation of surface waves by shear flows, *J. Fluid Mech., 6*, 568–582, 1959.

Mitsuyasu, H., and T. Honda, The high-frequency spectrum of wind generated waves, *J. Ocean. Soc. Jpn., 30*, 185–198, 1974.

Mitsuyasu, H., F. Tasai, T. Suhara, S. Misuno, M. Ohkuso, T. Honda, and K. Rindiishi, Observations of the directional spectrum of ocean waves using a cloverleaf buoy, *J. Phys. Oceanogr., 5*, 750–760, 1975.

Nickoleav, N. I., O. I. Yordanov, and M. A. Michalev, Non-Gaussian effects in two-scale model for rough surface scattering, *J. Geophys. Res., 97*, 15,617–15,624, 1992.

Phillips, O. M., The equilibrium range in the spectrum of wind generated waves, *J. Fluid Mech., 4*, 426–434, 1958.

Phillips, O. M., *The Dynamics of the Upper Ocean*, 2nd ed., Cambridge Univ. Press, New York, 1977.

Phillips, O. M., Spectral and statistical properties of the equilibrium range in the wind-generated gravity waves, *J. Fluid Mech., 156*, 505–531, 1985.

Pierson, W. J., The theory and applications of ocean wave measuring systems at and below the sea surface, on the land, from aircraft and from spacecraft, NASA contract report CR-2646, N76-17775, NASA, Washington, D. C., 1976.

Pierson, W. J., and L. Moskowitz, A proposed spectral form for fully developed wind sea based on the similarity theory of S. A. Kitaigorodskii, *J. Geophys. Res., 69*, 5181–5190, 1964.

Pierson, W. J., and R. A. Stacy, The elevation slope, and curvature spectra of a wind roughened sea surface, NASA contract report CR-2646, 126 pp., NASA, Washington, D. C., 1973.

Plant, W. J., A relationship between wind stress and wave slope, *J. Geophys. Res., 87*, 1961–1967, 1982.

Shemdin, H., and P. A. Hwang, Comparison of measured and predicted sea surface spectra of short waves, *J. Geophys. Res., 93*, 13,883–13,890, 1988.

Shemdin, H., M. Tran, and S. C. Wu, Directional measurement of short ocean waves with stereophotography, *J. Geophys. Res., 93*, 13,891–13,901, 1988.

Smith, J. A., Modulation of short wind waves by long waves, in *Surface Waves and Fluxes*, edited by G. L. Geernaert and W. J. Plant, pp. 247–284, Kluwer Acad., Norwell, Mass., 1990.

Smith, S. D., Coefficients for sea surface wind stress, heat flux, and wind profiles as a function of wind speed and temperature, *J. Geophys. Res., 93*, 15,467–15,472, 1988.

Smith, S. D., et al., Sea surface wind stress and drag coefficients: The HEXOS results, *Boundary Layer Meteorol., 60*, 109–142, 1992.

Sobieski P., C. Baufays, A. Guissard, P. Siraut, and A. Vander Vorst, Study on propagation and inverse scattering, ESA ESTEC contract 5285/82 report, Eur. Space Agency, Eur. Space Res. and Technol. Cent., Noordwijk, Netherlands, March 1986.

Sobieski P., C. Baufays, A. Guissard, P. Siraut, and A. Vander Vorst, Study of propagation models for maritime missions, ESA ESTEC contract 5971/84/NL/GM report, Eur. Space Agency, Eur. Space Res. and Technol. Cent., Noordwijk, Netherlands, Feb. 1988.

Toba Y., Local balance in the air-sea boundary processes, III, On the spectrum of wind waves, *J. Oceanogr. Soc. Jpn., 29*, 209–225, 1973.

Wilson, B. W., Numerical prediction of ocean waves the North Atlantic for December 1959, *Dtsch. Hydrogr. Z., 18*, 114–130, 1965.

Wu, J., Sea-surface slope and equilibrium wind-wave spectra, *Phys. Fluid, 15*, 741–747, 1972.

Wu, J., Wind stress coefficients over sea surface from breeze to hurricane, *J. Geophys. Res., 87*, 9704–9706, 1982.

Wu, J., Mean square slopes of the wind-disturbed water surface, their magnitude, directionality, and composition, *Radio Sci., 25*, 37–48, 1990.

Wu, J., Near-nadir microwave specular returns from the sea surface—Altimeter algorithms for wind and wind stress, *J. Atmos. Oceanic Technol., 9*, 659–667, 1992.

Young, I. R., L. A. Verhagen, and M. L. Banner, The evolution of wind generated waves in water of finite depth, paper presented at 2nd International Conference on Air-Sea Interaction and Meteorology and Oceanography of the Coastal Zone, Am. Meteorol. Soc., Lisbon, Portugal, 1994.

Zhang, X., Capillary-gravity and capillary waves generated in a wind wave tank: Observations and theories, *J. Fluid Mech., 289*, 51–82, 1995.

B. Chapron, T. Elfouhaily, and K. Katsaros, IFREMER Centre de Brest, B.P. 70-29280 Plouzane cedex, France. (e-mail: tanos.el.fouhaily@ifremer.fr)

D. Vandemark, NASA GSFC, Wallops Flight Center, Laboratory for Hydrospheric Processes, Bldg. N159, Wallops Island, VA 23337. (e-mail: dug@aol7.wff.nasa.gov)

(Received April 9, 1996; revised September 20, 1996; accepted January 3, 1997.)